Assessment of a damage model for wound composite structures by acoustic emission

Juan Pedro Berro Ramirez Berro Ramírez, Damien Halm, Jean-Claude Grandidier

ASSESSMENT OF A DAMAGE MODEL FOR WOUND COMPOSITE STRUCTURES BY ACOUSTIC EMISSION

Juan Pedro Berro Ramirez [1], Damien Halm[2*], Jean – Claude Grandidier[2]

[1]Altair Engineering France, 92160 ANTONY Cedex - France
[2]Institute Pprime (UPR 3346), CNRS – ENSMA – Université de Poitiers, BP40109, 86961 FUTUROSCOPE CHASSENEUIL CEDEX – France
* *corresponding author :* damien.halm@ensma.fr

Key words: Damage Model, Acoustic Emission, Finite Element Analysis, Wound Composite.

Abstract. This paper deals with the link between the acoustic activity due to damage in wound composite structures and the simulated evolution of damage variables. A damage model able to accurately capture the different degradation modes which may occur in this type of material is first selected. A parallel is drawn between the continuous evolution of the damage variables and the discrete acoustic events. The mechanical behavior of notched samples made of two different wound composite lay-ups and involving complex damage combinations are simulated and compared to acoustic emission. The satisfactory correlation confirms the physical meaning of the damage variables and validates the model assumptions. The association of experimental acoustic signals and a damage model is a tool to understand the degradation scenario of wound composite structures and the meaning of the recorded acoustic events.

1 INTRODUCTION

Composite materials (CFRP) can exhibit various damage mechanisms (matrix cracking, fiber / matrix debonding, fiber breakage, delamination,…) which lead to

mechanical properties' degradation and potentially final failure of the structure. Several approaches attempt to predict failure of composite structures by using fracture criteria ([1,2] among many others). Xu et al [3] compare the capability of these simple criteria to predict composite pressure vessel burst. These approaches, in their initial version, provide only binary indications (failed / not failed) and do not capture the progressive nature of these phenomena. One alternative to simulate any material damage process, and in particular its progressiveness, is the Continuun Damage Mechanics. For several years, a large number of damage models have been developed for multiple applications, from the ductile materials to quasi – brittle behaviour. The framework of Continuum Damage Mechanics has considerably evolved since the pioneering works of Kachanov [4] . This formalism has proved its advantages in different applications, as it can be seen in the work by Chaboche [5], Krajcinovic [6] or Talreja et al. [7] among many others. Numerous models written in this framework are dedicated to composite materials (specifically CFRP). For example, some models focus on microscopic scale. These models study the different material constituents like fibers, matrix, interfaces [8,9]. Other models focus on the "mesoscale", namely the ply scale [10-16]. This class of models proved to provide excellent results in the WWFE (World Wide Failure Exercise, [17,18]).

In general, the damage evolution law is identified and validated by comparison of experimental mechanical response and damage observations with simulated ones. As the loss of stiffness is the main mechanical signature of damage, the measure of the change in elasticity is commonly used to identify the evolution laws of the variables [19]. Another technique which is more and more used to study damage in composite materials is the Acoustic Emission monitoring. Acoustic waves are generated in solids

by the rapid release of strain energy [20]. For example, a crack growth releases a given quantity of elastic energy. AE monitoring is the detection of these elastic waves due to damage growth. The high sensitivity of AE testing, coupled with its need for relatively few sensors, make it an attractive technique. It has been extensively used and assessed as an alternative damage measurement technique [21-23]. One sensor allows one recording the acoustic signals. With at least two sensors, it is possible to locate the source of the echoes [24,25]. This is an advantage for large composite structures, such as wind turbine blades [26,27]: in spite of the scale difference (defects of a few centimetres in a blade whose length is several tens of meter), AE monitoring can successfully provide early warning of damage onset and propagation. It also makes possible to distinguish between the damage modes by the use of cluster analysis together with classification techniques [28-30].

The acoustic emission is directly related to the damage phenomena occurring in the composite material. In the view of determining the mechanical strength of filament-wound pressure vessels, Mahdavi et al. [31] proved the acoustic parameters (energy, accumulated energy, amplitude,…) can be used to describe the failure mechanisms in ring specimens subjected to hoop tensile stress. Blassiau et al. [32] compared the number of accumulated acoustic events with model predictions of fibre breakage in a unidirectional composite and proposed a tool to assess the lifetime of hydrogen vessels subjected to constant inner pressure. These works show the direct link between damage and acoustic activity in complex composite structures such as wound tanks. The objective of this work is to correlate AE to the evolution of internal variables in order to reinforce their physical meaning. The damage model selected here has been proposed by Berro Ramirez et al. [33] and is dedicated to the simulation of degradation

mechanisms observed in wound composite pressure vessels. It assumes the failure is the result of the combination of elementary damage modes quantified by internal variables and whose effects are assembled in the expression of the constitutive relation through the tensorial functions representation theory. Showing the simulated damage evolution matches the acoustic events is a mean of validating the model assumptions and of proving that it is capable of simulating the behavior of complex composite structures. Such equivalences have been addressed in the literature but in general with simpler models that do not distinguish the different modes of damage [34].

This work highlights the parallel between the damage variables of a Continuum Damage Mechanics (CDM) model (which are the outputs of a Finite Element analysis and are considered as “virtual” acoustic echoes) and the measured acoustic energy. This comparison needs two tools:

- a damage model, which has to simulate accurately all the damage modes undergone by wound composite structures and their consequences on the stiffness. Section 2 briefly recalls the outlines of the model developed by Berro Ramirez et al.[33] for wound composite materials. It is based on the concepts of CDM and has been used to simulate the behavior of notched structures and finally applied on pressure vessel burst simulations [35].
- a procedure to link damage evolution (a continuous process) and acoustic emission (discrete events) from tests involving only one damage mode. Section 3 specifies the “virtual” acoustic emission procedure, its implementation and identification.

Section 4 presents the comparison between the simulated acoustic signals and the experimental results obtained from tensile tests carried out on two types of specimens

($[\pm 45_4]_s$ and a quasi-isotropic sequence $[0_2, \pm 45_2, 90_2]_s$) representative of the structure of wound composite vessels and involving complex spatial and temporal combinations of damage modes. This comparison aims to validate the model's ability to simulate damage and its consequences accurately not only at the macroscopic scale (tensile failure load, elasticity change, see Berro et al. [35]) but also at mesoscopic scale (local damage mechanisms evidenced by acoustic emission).

2 OUTLINES OF THE DAMAGE MODEL

This section summarizes the main features of the damage model which has been developed to simulate the behavior of wound composite vessels subjected to inner pressure [35]. A more detailed presentation can be found in [33].

- Damage mechanisms

The damage modes activated in the composite shell of wound pressure vessels are of two types:

(i) brittle fracture (fibre failure, fibre – matrix interface failure and delamination),

(ii) progressive degradation due to fibre matrix debonding and matrix microcracking (the so called diffuse damage [10]).

Two additional phenomena are incorporated in order to get a better representation of the composite behaviour when subjected to shear loading, namely matrix viscosity and permanent shear strain.

- Fixed directions approach – internal variables

The model is built in the framework of the Continuum Damage Mechanics using the concepts and tools of the Thermodynamics of Irreversible Processes. The model has to simulate the mechanical behaviour of composite structures undergoing the following phenomena:

- non linear degradation of the stiffness due to the various damage mechanisms
- initial and damage induced anisotropy
- permanent shear strain and viscosity

To build the model, the fixed damage directions concept based on the work by Boelher [36] is used. According to [37], it is supposed that every damage state (anisotropic by nature) is decomposed, at the meso – scale (*i.e.*, at the ply scale), in a set of couples $\left(\rho_i, \overline{\overline{N}}_i\right)$, whose number is to be defined. The fixed directional $\overline{\overline{N}}_i$ tensors are defined as $\overline{\overline{N}}_i = \overline{n}_i \otimes \overline{n}_i$, where $\overline{n}_i$ is the normal to the fracture surface and is related to the aforementioned damage modes. These directions are chosen according to the material anisotropy. Damage growth is represented by the evolution of the scalar damage internal variables ρ_i associated to the corresponding damage system. These damage variables evolve from 0 (for a sound material) to 1 (maximum damage).

- Choice of the damage systems

At the ply scale, the $\overline{n}_i$ vectors allowing to build the directional tensors $\overline{\overline{N}}_i$ associated to the damage modes are respectively $\overline{n}_0$ (fibre direction), $\overline{n}_{90}$ (normal to the fibre direction), $\overline{n}_{HP}$ (normal to the ply) and $\overline{n}_{i-j}$ (at 45° of the direction *i* and *j*). These vectors are represented in Figure 1, according to [33].

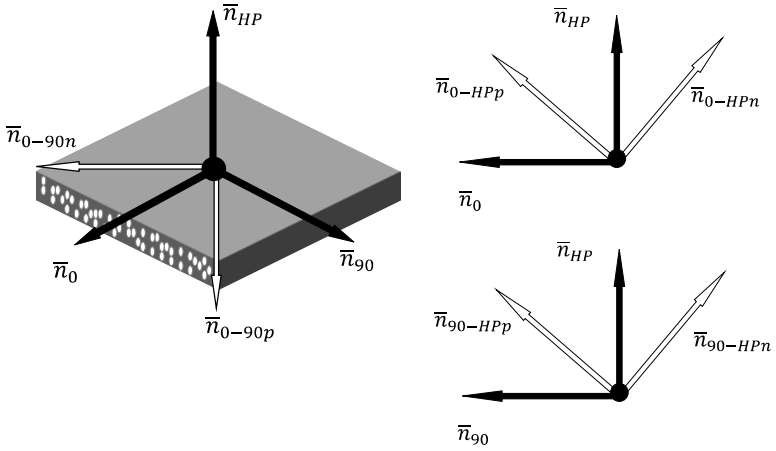

Figure 1: Damage systems at the ply scale

From these vectors, four sets of directional tensors are considered:

- $\overline{\overline{\mathrm{N}}}_0$ related to fibre direction and fibre fracture. The scalar variable associated is ρ_0
- $\overline{\overline{\mathrm{N}}}_{90}$ related to transverse direction and associated to fibre – matrix interfaces fracture in tension. The corresponding variable is ρ_{90}.
- $\overline{\overline{\mathrm{N}}}_{\mathrm{HP}}$ related to the direction normal to the ply plane and associated to delamination phenomena (Mode I). Its scalar damage variable is ρ_{HP}.
- $\overline{\overline{\mathrm{N}}}_{\mathrm{i-j\,p/n}}$ (*i* and *j* take the values 0, 90 and HP: $\overline{\overline{\mathrm{N}}}_{0-90\,\mathrm{p}}$, $\overline{\overline{\mathrm{N}}}_{0-90\,\mathrm{n}}$, $\overline{\overline{\mathrm{N}}}_{0-\mathrm{HP\,p}}$, $\overline{\overline{\mathrm{N}}}_{0-\mathrm{HP\,n}}$, $\overline{\overline{\mathrm{N}}}_{90-\mathrm{HP\,p}}$, $\overline{\overline{\mathrm{N}}}_{90-\mathrm{HP\,n}}$) related to shear directions (+45° (p) and -45° (n)) with respect to i-th direction. These directional tensors are associated to so-called diffuse damage (that is to say, matrix micro – cracking, fibre – matrix debonding, delamination (mode III) in 0° - 90° directions and delamination (mode II) in 0°/90° – HP directions) related to shear loadings, permanent shear

strain and matrix viscosity. The scalar damage variable associated to diffuse damage is noted ρ_s in the following.

The permanent strain, due to irreversible sliding of cross-plies (visible in particular on [±45] samples) is assumed to be the sum of elementary sliding contributions γ_+ and γ_- which are activated by in-plane shear strains and are associated respectively to the directions $\overline{\overline{N}}_{0-90\,p} - \overline{\overline{N}}_{0-90\,n}$ and $\overline{\overline{N}}_{0-90\,n} - \overline{\overline{N}}_{0-90\,p}$. The global permanent strain tensor $\overline{\overline{\Psi}}$ adds the contribution of the elementary sliding variables. Regarding the viscous behaviour (attributable to the matrix and which can be observed under shear), it is represented by a set of scalar variable z_{0-90}, z_{0-HP} and z_{90-HP} associated to the in-plane and out-of-plane shear directions. The global viscous variable $\bar{\bar{Z}}$ contains the contribution of each elementary variable z_{i-j}.

- Thermodynamic potential

The tensorial functions representation theory [36] is a guide to build the thermodynamic potential (strain energy per unit volume, noted w in the following) from tensorial invariants. At the ply scale, three parts can be distinguished: an elastic contribution w_{Elastic}, a damage term w_{Damage} involving each damage variable ρ_i and the viscous contribution w_{viscous}.

$$w\left(\bar{\bar{E}}, \overline{\overline{N}}_0, \overline{\overline{N}}_{90}, \overline{\overline{N}}_{HP}, \left\{\overline{\overline{N}}_{i-j\,p/n}\right\}, \bar{\bar{Z}}, \{\rho_i\}\right) = \tag{1}$$

$$w_{Elastic}\left(\bar{\bar{E}}, \overline{\overline{N}}_0\right) + w_{Damage}\left(\bar{\bar{E}}, \overline{\overline{N}}_0, \overline{\overline{N}}_{90}, \overline{\overline{N}}_{HP}, \left\{\overline{\overline{N}}_{i-j\,p/n}\right\}, \{\rho_i\}\right) + w_{Viscous}\left(\bar{\bar{E}}, \left\{\overline{\overline{N}}_{i-j\,p/n}\right\}, \bar{\bar{Z}}\right)$$

where $\overline{\overline{E}}$ the elastic strain tensor, which is the difference between the total strain $\bar{\bar{\varepsilon}}$ and the permanent strain tensor $\bar{\bar{\Psi}}$ defined as:

$$\bar{\bar{\boldsymbol{E}}} = \bar{\bar{\boldsymbol{\varepsilon}}} - \bar{\bar{\boldsymbol{\Psi}}} = \bar{\bar{\boldsymbol{\varepsilon}}} - \left[\boldsymbol{\gamma}_{+}\left(\bar{\bar{\boldsymbol{N}}}_{\boldsymbol{0-90p}} - \bar{\bar{\boldsymbol{N}}}_{\boldsymbol{0-90n}}\right) + \boldsymbol{\gamma}_{-}\left(\bar{\bar{\boldsymbol{N}}}_{\boldsymbol{0-90n}} - \bar{\bar{\boldsymbol{N}}}_{\boldsymbol{0-90p}}\right)\right] \quad (2)$$

In Equation (1), $\left\{\bar{\bar{N}}_{i-j\,{}^{p}/_{n}}\right\}$ and $\{\rho_i\}$ stand for the set of shear directional tensors and the set of damage variables, respectively. As the initial ply is transversely isotropic, the corresponding elastic potential is built using only the directional tensor $\overline{\overline{N}}_0$ [38]. The detailed expressions of $w_{elastic}$, w_{Damage} and $w_{Viscous}$, built from the theory of tensorial functions representation, can be found in [33].

- Reversibility domains and evolution laws

According to the Thermodynamics of Irreversible Process, the elastic stress $\bar{\bar{\sigma}}$ and the thermodynamic forces $F_{\rho_i}, F_{\gamma_+}, F_{\gamma_-}$ and $F_{z_{i-j}}$ associated to each internal variable (ρ_i, γ_+, γ_- and z_{i-j} respectively) are obtained by deriving w:

$$\bar{\bar{\sigma}} = \frac{\partial w}{\partial \bar{\bar{E}}} \quad F_{\rho_i} = -\frac{\partial w}{\partial \rho_i} \quad F_{\gamma_+} = -\frac{\partial w}{\partial \gamma_+} \quad F_{\gamma_-} = -\frac{\partial w}{\partial \gamma_-} \quad F_{z_{i-j}} = -\frac{\partial w}{\partial z_{i-j}} \quad (3)$$

The evolution of the internal variables is found to follow the normality rule with respect to the elastic domain. The general expression of the reversibility domain associated to each internal variable reads:

$$\boldsymbol{f}_{\boldsymbol{\rho_i}}\left(\boldsymbol{F}_{\boldsymbol{\rho_i}}, \boldsymbol{\rho_i}\right) \leq \boldsymbol{0},\ \boldsymbol{f}_{\boldsymbol{\gamma}}\left(\boldsymbol{F}_{\boldsymbol{\gamma_\pm}}, \boldsymbol{\gamma_\pm}\right) \leq \boldsymbol{0} \quad (4)$$

According to the damage evolution type, the threshold function $f_{\rho i}$ takes different forms [33]: it is a linear function of the thermodynamic force is the case of a brittle behaviour, whereas it tends towards an asymptote for a more progressive damage. Regarding the threshold of the shear permanent strains γ_+ and γ_-, a function linear with respect to the corresponding thermodynamic force is selected. The normality rule, associated to the threshold function, is found to be flexible enough to simulate both types of damage evolution (brittle and progressive) and the permanent strain evolution.

Unlike damage, viscosity is assumed not to be limited by a threshold function but to occur as soon as a shear strain is applied, the evolution of the variables $z_{i\text{-}j}$ is directly proportional to the corresponding thermodynamic force. The detailed expressions of the threshold functions, as well as that of the thermodynamic potential and the evolution laws can be found in [33]. Note that a probabilistic version of this model taking into account the statistical material strength distribution can be found in [39]. The variability sources are the random failure of the fiber and the volumetric fraction of fibers. For the sake of simplicity, only the deterministic version is used in this paper.

The model is first implemented in the Finite Element software ABAQUS by the means of a subroutine UMAT, which allows to simulate any mechanical behaviour of a structure by using a specifically designed model. In a second step, this UMAT subroutine is used to identify the model parameters by simulating tensile loadings performed on three different types of specimens made from wound pipes ($[0_8]$, $[90_8]$, $[\pm 45_4]_s$). These tubes are first manufactured by filament winding on a cylindrical mandrel. Two types of plies are manufactured: circumferential plies used for layers oriented at 0 ° and 90 ° (with no interlacing) and helical plies with interlaced fibers. The tubes are then cut along the shaft and laid down flat. The plates the samples are taken

from are made by stacking these elementary wound plies, after which they are placed in a vacuum bag and cured in an autoclave (see [40] for details about manufacturing of these samples).

3 "VIRTUAL" ACOUSTIC EMISSION

The acoustic emission, whose principles have been briefly recalled in Section 1, allows one getting a qualitative assessment of the damage onset and its location in the studied structure. It is also a way to validate and emphasize the capabilities of the damage model presented in the previous section by associating virtual echoes (*i.e.*, simulated damage evolution) to each damage event experimentally recorded. A parallel is drawn between these virtual echoes and the acoustic energy measured by sensors during tensile tests performed on flat specimens.

These virtual echoes are "listened" (actually, simulated) by using a specific type of variable in an ABAQUS UMAT subroutine. Three different echoes are used to simulate the global acoustic signal. These echoes are associated to (i) fiber breakage (damage variable ρ_0), (ii) matrix / fiber interface fracture (damage variable ρ_{90}) and (iii) diffuse damage (damage variable ρ_s). Note that out–of–plane damage is ignored: the tensile test performed on flat samples will be simulated in a 2D framework (samples are meshed with shell elements). However, echoes related to out–of–plane damage could be easily introduced in the numerical procedure.

In the framework of a CDM model, the material stiffness is weakened by damage variables whose evolution is supposed to represent the succession of degradation events. These variables progressively increase (more or less rapidly) and, in the same way, the

acoustic events (each characterized by a given energy level) appear from a low strain level and are cumulative until final fracture. The key aspect of this work is to link simulated damage evolution and acoustic events: it is necessary to assign an energy signature to each modeled damage mode. To this end, tensile tests are performed on parallelepipedic (250mm x 25mm x 2mm) $[\pm 45_4]_s$ samples cut from wound composite pipes. The material is a prepreg composite composed of Toray T700SC fibres and a TCR UF3369 thermoset epoxy matrix. The acoustic acquisition set-up is composed of two piezo-electric sensors Micro80 (with a silicon grease couplant) and of a PCI-2 system from Mistras Group with a detection threshold of 35dB. The preamplifier gain is 40dB. Figure 2 displays a schematization of these tests.

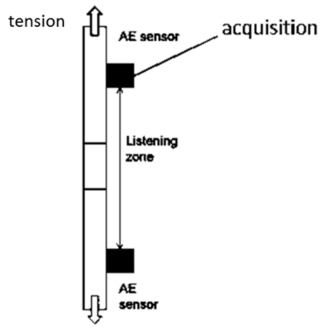

Figure 2: Experimental device: mechanical loading and acquisition of acoustic signals

From these tests, diagrams plotting acoustic energy vs. time are obtained and analyzed. As an example, Figure 3 displays diagrams recorded during a tension test performed on a $[\pm 45_4]_s$ sample [40].

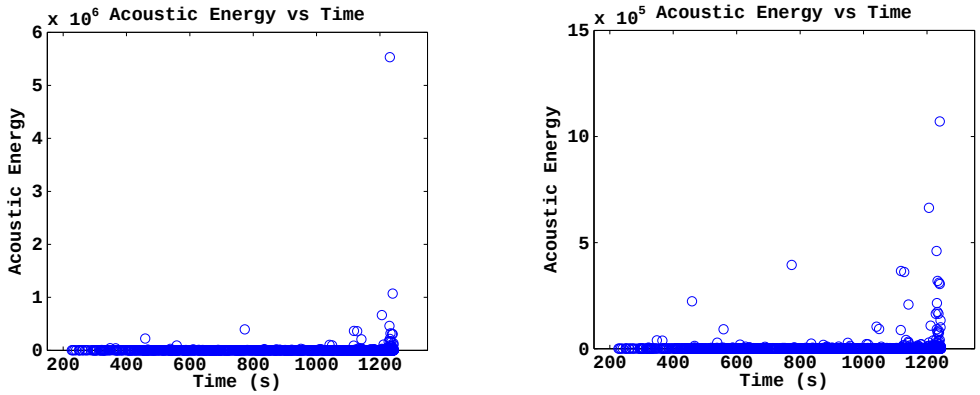

a b

Figure 3. a) Acoustic energy (unit: aJ, 1aJ = 10^{-18}J) vs. time of the tension test. b) Zoom in on the middle and low energy ranges.

These two curves clearly exhibit the predominance of low and intermediate energy echoes which can be associated to diffuse and fibre / matrix interface damage, as pointed out on a similar material in Bertin [41]. Fibre breakage is characterized by much more energetic events, which can be observed at the right side of Figure 3a, at the very end of the test. Consequently, it appears reasonable to choose three energy levels: a low energy level, associated to diffuse damage (points at the bottom of Figure 3b), an intermediate one, associated to fibre / matrix interface damage (visible in particular between 1000s and 1200s), and a high one corresponding to the fibre breakage.

Once the number of energy levels has been chosen, it is necessary to link a discrete phenomenon (the acoustic signal) to a continuous one (the damage variable evolution for each damage mode). A possible way to make this association is to emit one virtual echo when the damage variable reaches the maximum value ρ_i = 1 (or a lower value). However, this method is not very realistic because some phenomena (such as fibre / matrix debonding, diffuse matrix cracking, breakage of isolated fibres) are progressive by nature and can generate several echoes before the damage variable has reached its maximum value. The method chosen here is based on a pseudo – discrete acoustic

emission, which is a compromise between a discrete event and a continuous process. A set of n arbitrary damage values (ρ_{i-1}, ρ_{i-2},…, ρ_{i-n}) is selected and at each value the corresponding simulated strain level ($\varepsilon_1^{\rho_i}$, $\varepsilon_2^{\rho_i}$,…,$\varepsilon_n^{\rho_i}$) is recorded (see in Figure 4 a schematisation of a damage variable evolution curve). An energy level S_1, S_2,…, S_n is assumed to be released as soon as strain reaches the aforementioned values. This principle is illustrated in Figure 4. The cumulated energy (acoustic energy cumulated over the time), which is one of the standard post-processing coming from experimental data, is thus used in this study. From the FE point of view, the energy level corresponding to each numerical acoustic energy release is stored and cumulated in a history variable, which means that for each time step the energy released by all integration points is added to the former value. This way to store the acoustic energy allows to compare directly with experimental data.

In this case, without loss of generality, three damage levels are chosen for the variable ρ_i (*i.e.*, for a given damage mechanism). Consequently, the acoustic energy is assumed to be released in a stepwise manner with three different levels S_1, S_2 and S_3. The values $\varepsilon_I^{\rho_i}$ and $\varepsilon_F^{\rho_i}$ stand for the strain at damage onset and at maximum damage, respectively.

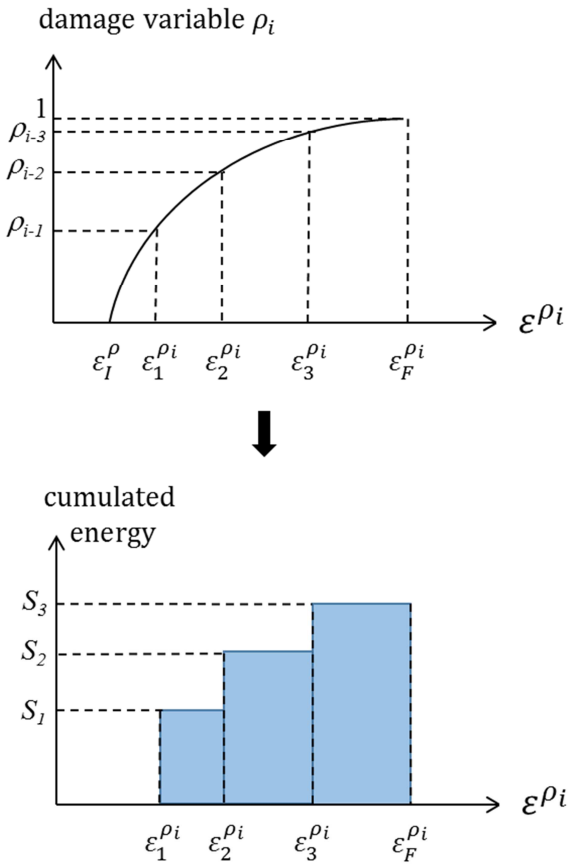

Figure 4. Link between progressive damage evolution / discrete energy release.

The choice of the number of damage levels is arbitrary but it must match the damage progressiveness: the more progressive the damage evolution, the higher n.

It is now necessary to define the energy values S_1, S_2 and S_3. The starting point is the total energy released by the considered damage mechanism. This energy value is chosen according to the experimental records in Figure 3: in the order of 10^6aJ for fiber, 10^4aJ for matrix cracking and 10^2aJ for diffuse damage. Each intermediate energy level S_j (with j=1,2,3) is defined as the total energy of the event type (noted S in Equation 5) weighted by the corresponding strain range normalized by the total strain range of acoustic activity $[\varepsilon_1^{\rho_i}, \varepsilon_F^{\rho_i}]$:

$$S_j = S\frac{\varepsilon_{j+1}^{\rho_i} - \varepsilon_j^{\rho_i}}{\varepsilon_F^{\rho_i} - \varepsilon_1^{\rho_i}} \quad (5)$$

where the strain values $\varepsilon_j^{\rho_i}$ and $\varepsilon_{j+1}^{\rho_i}$ are the bounds of the *j*-th energy interval determined from the selected damage levels $\rho_{i\text{-}j}$ (Figure 4). For the n-th (last) interval, $\varepsilon_{n+1}^{\rho_i}=\varepsilon_F^{\rho_i}$.

This method is applied to identify the values of the acoustic energy associated with the three damage modes: fiber breakage, fiber / matrix interface failure and diffuse damage. Acoustic data from two different tests are used in order to identify the different energy levels. It is important to keep in mind the qualitative nature of this approach. These two tests are:

- Tensile test on $[\pm 45_4]$s samples, characterized by an early initiation of the diffuse damage, followed by a contribution of the fiber / matrix interface failure. The results are presented in Figure 3.
- Tensile test on a sample containing fibers oriented at 0°. Here, data from notched $[0_2, \pm 20_2]_s$ samples have been selected, which undergo fiber breakage (Figure 5).

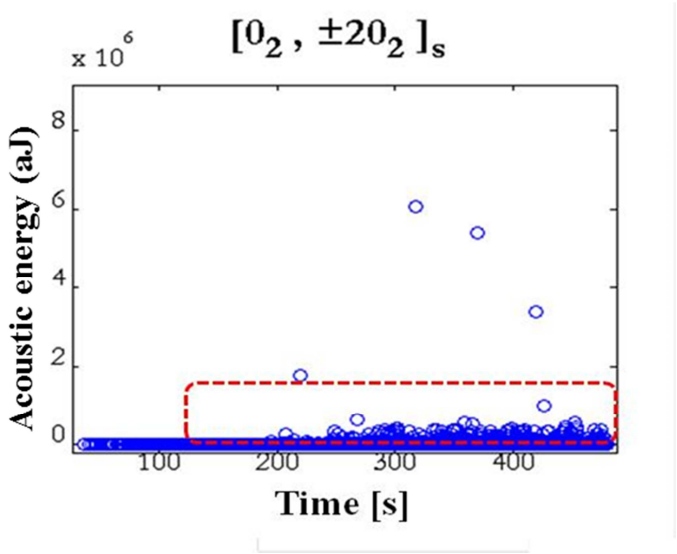

Figure 5: Acoustic energy vs. time recorded during a tension test on a notched $[0_2, \pm 20_2]_s$ sample

In order to identify the fiber breakage signature, echoes located in the red rectangle are considered as the ones associated with isolated fiber failure rupture. At the end of the test (close to final fracture), clusters of fibers begin to break releasing extremely energetic signals. Regarding diffuse damage and fiber / matrix interface failure, the two corresponding energy levels can be distinguished in Figure 3: a very low level (a few hundreds of aJ) for diffuse damage and a intermediate level (a few tens of thousands of aJ) for interface failure. Finally, the selected values are presented in Table 1:

Damage mode	Number n of intervals	Damage values	Acoustic energy [aJ]
Fiber breakage	3	$\rho_1 = 0.5$ $\rho_2 = 0.7$ $\rho_3 = 0.8$	5.75E3 4.40E5 1.20E6
Fiber / matrix failure	1	$\rho_1 = 0.1$	4.0E4
Diffuse damage	4	$\rho_1 = 0.2$ $\rho_2 = 0.4$ $\rho_3 = 0.5$ $\rho_4 = 0.54$	407 463 517 611

Table 1: Selected damage values and corresponding acoustic energy values

One can observe in this table that:

- fiber / matrix interface failure is associated to only one acoustic level. This choice is justified by the brutal onset and propagation of the kind of damage and seems to be well suited to this type of energy release
- the damage levels for fiber breakage are chosen such that energy is released in the last stages
- the energy release by diffuse damage is supposed to be more uniformly distributed.

The method presented above is able to simulate the virtual acoustic emission at one material point of the structure: indeed, in a Finite Element approach, the damage evolution (and equivalently the acoustic emission) is calculated at each integration point of the structure. However, as the acoustic sensors in the experiment schematized in Figure 2 record the events that occurred in the whole sample, it is necessary to compare these experimental data with a variable representing the sum of all virtual signals emitted at each integration point. To this end, the UMAT subroutine allows to use a

specific variable, called SCD, which has the ability to sum the contributions of all finite elements in a given increment of time. This variable is originally dedicated to the calculation of creep dissipated energy, but its use is here modified so that it represents, at each time integration, the sum, in the whole structure, of the simulated energy echoes energies emitted by fiber breakage, fiber / matrix interface debonding and diffuse damage respectively.

4 SIMULATION OF THE ACOUSTIC EMISSION IN WOUND COMPOSITE SAMPLES SUBJECTED TO TENSION

The simulation of the acoustic emission in wound composite structures is compared with the experimental energy recorded during tensile tests performed on notched samples. The geometry of these notched wound composite samples is given in Figure 6. These experimental results come from a test campaign performed on different types of samples [40]. Note that although flat these notched samples have been manufactured by filament winding, in the same way as those used to identify the acoustic energy related to the damage evolution (previous section), and then cut by water jet.

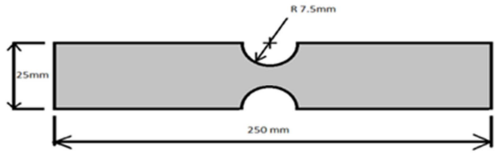

Figure 6: dimensions of the notched samples

The acoustic emission related to damage has been simulated for two different stacking sequences: a simple $[\pm 45_4]_s$ lay-up and a more complex quasi-isotropic one ($[0_2, \pm 45_2, 90_2]_s$). The thickness of one layer is about 0.22 mm.

The mechanical and acoustic behaviour has been simulated by the means of the FE software ABAQUS. Due to the small thickness, the samples are meshed by two-dimensional shell elements (7708 triangle quadratic shell element with reduced intergration). Regarding the boundary conditions, a constraint (zero-displacement) has been imposed on one end and a progressively increasing displacement on the other one with a speed of 0.5 mm/min.

4.1 Results of tensile test on $[\pm 45_4]_s$ sample

In order to compare the experimental and simulated acoustic signals, the interferences occurring at the end of the test (acoustic post-failure emissions) have been removed as they do not convey information on the initiation and evolution of damage. In addition, the test duration and the cumulative energy have been normalized in order to compare the shape of the curves. This curve processing eases the comments of the changes in the slopes and allows to draw a parallel between the acoustic energy and the different damage modes. The comparison is shown in Figure 7.

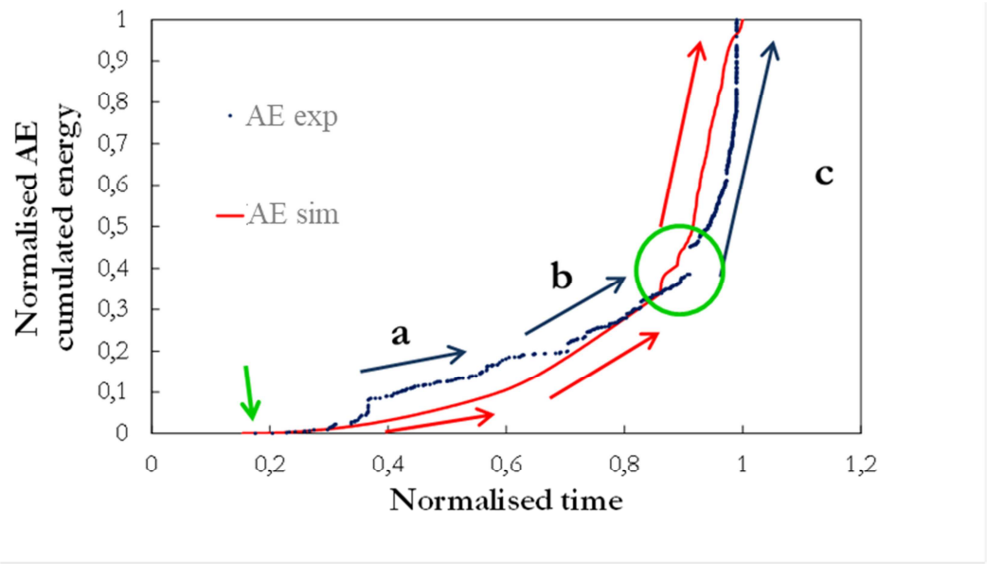

Figure 7. Comparison experimental and simulated acoustic emission for a $[\pm 45_4]$s notched wound composite sample

Some interesting details can be observed in this figure. Firstly, the beginning of the acoustic emission is identical in both cases (experiment and simulation, see green arrow). This fact emphasizes the relevance of the procedure proposed in [33] to identify the threshold of the diffuse damage (the first one which appears in the damage sequence): it is determined from the stiffness decrease observed on cyclic tension tests performed on [±45] samples.

Note also that the changes of the slope of the experimental curve are fairly well simulated by the model (red and blue arrows). As only diffuse damage evolves and generates acoustic emission in this period of time, these successive changes of slope have to be explained by the specific evolution of this damage variable (Figure 8 displays the diffuse damage configuration simulated by the CDM model):

- in Part ***a*** of the curve, only a small zone of the sample in the vicinity of the notch undergoes diffuse damage (see Figure 8a) and therefore it emits energy signals. However, this damage evolution (and consequently the simulated acoustic emission) is limited: as specified in Section 2, the choice of the reversibility domain for the diffuse (progressive) damage leads to asymptotic evolution and the damage level cannot exceed a given value.
- when damage in the neighborhood of the notch is close to saturation, diffuse damage starts to spread in the areas of the specimen located on both sides of the notch (Figure 8b). This spatial extension explains the change of slope at the beginning of Part ***b***. Thus, changes in slope of cumulative energy curves may indicate an increase in the size of the damaged area and not the onset of another type of damage.
- at the end of Part ***b*** (in the simulated curve), an acceleration of the acoustic energy can be noticed: it corresponds to the onset of fiber / matrix interface debonding and not to diffuse damage growth since this degradation mode has spread throughout the sample and reached its maximum value (Figure 8c). The presence of this acceleration is validated by the occurrence of a jump at the same time on the experimental curve before the sudden and quick increase of energy leading to final failure.

Note that, beyond the identification of the energy levels presented in Section 3, the simulation of the $[\pm 45_4]_s$ samples is a good way to interpret the different regimes which are observed on the acoustic energy curve and to related them to damage in specific zones.

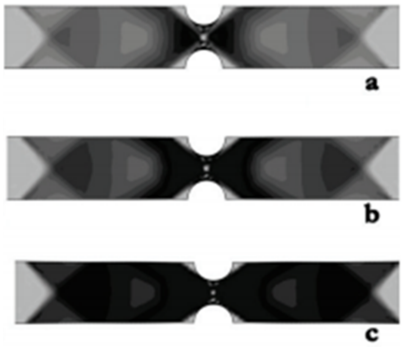

Figure 8: Simulated diffuse damage level during phases a, b and c of the acoustic emission curve (the darker the color, the higher the damage level)

4.2 Results of tensile test on $[0_2, \pm45_2, 90_2]_s$ sample

In the same way as for the [±45] samples, the acoustic emission is recorded during tensile tests performed on quasi-isotropic samples (made of the same material and manufactured in a similar way) and compared to the corresponding simulation.

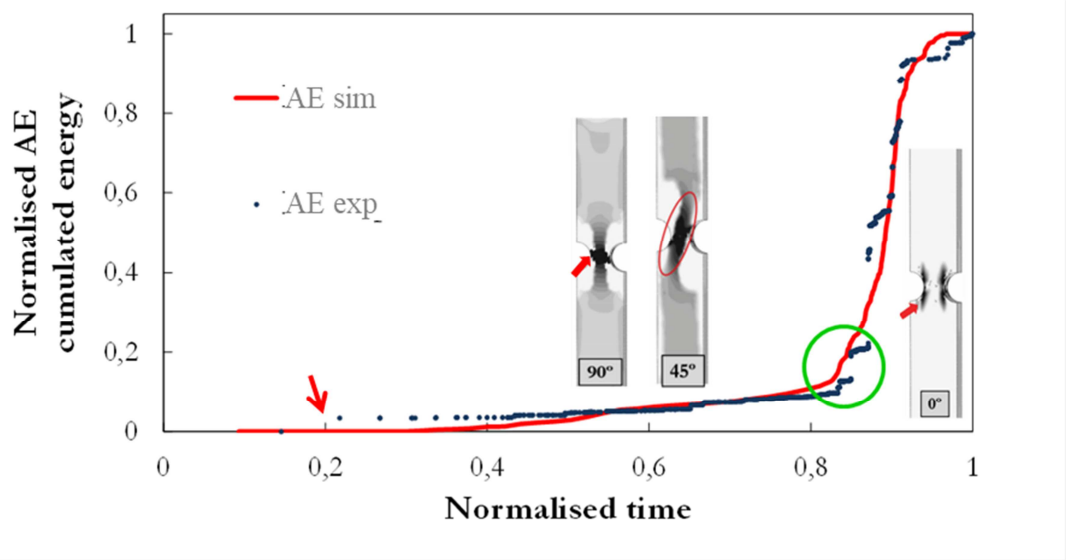

Figure 9: Comparison between experimental and simulated acoustic emission for a quasi-isotropic $[0_2, \pm 45_2, 90_2]_s$ notched wound composite sample – simulated configuration of fiber / matrix debonding and diffuse matrix cracking in the 0°, 45° and 90° plies (the darker the color, the higher the damage level)

A good agreement is also found for this sample between the simulated acoustic energy and the experimental one recorded during the test. While experimental acoustic emission starts at a normalized time of about 0.2 (red arrow), the simulation predicts a later onset, at 0.4. As shown on the simulated damage configuration in Figure 9, in a first stage, the simulated energy increases because of the contribution of fiber / matrix interface debonding in 90° plies and the diffuse damage in 45° cross plies. The simulations show these damage zones are mainly located in the vicinity of the notch. Matrix cracking is also found in the 0° plies: this splitting phenomenon is a precursor of fiber breakage, which starts when the slope suddenly increases at a normalized time of about 0.85 (marked by a green circle) and leads to a rapid final failure. The model

captures in a satisfactory way the onset of more energetic events: the slope change of the simulated curve exactly coincides with jumps in the experimental records due to the first fiber failure. In the last part of the test, experimental and simulated curves exhibit the same slope and it is worth noting that the model is also able to simulate the energy saturation in the very last step of the test, in accordance with experiment.

6. CONCLUSION

This paper has investigated a way to link the acoustic activity due to damage in wound composite structures subjected to monotonic loading and the simulated evolution of damage variables. This correlation is made possible thanks to a model able to accurately capture the different damage modes which may occur in this type of material (fiber breakage, diffuse matrix microcracking, fiber / matrix debonding). A specific methodology draws the parallel between the damage variables (whose evolution is by nature continuous) and the discrete acoustic events, by defining a given number of load intervals associated to given energy levels. This approach allows simulating the succession of the different acoustic events (*i.e.*, the emission onset, the transition between different types of events,…) and interpreting the damage kinetics (activation / deactivation of damage modes, spatial extension of damaged areas,…). The damage model parameters are identified only from mechanical tests. Regarding identification, two ways to improve it can be discussed, although the agreement between damage and acoustic activity is satisfactory. The first one consists of inverse characterization through optimization method in order to fit the acoustic signatures of each damage

mode. Other laminate sequences could be interesting to perform this kind of identification, like $[0,90]_s$ laminates, where matrix transverse cracks can evolve without causing the coupon's catastrophic failure. With such kind of samples, both fibers rupture and transverse cracks can be identified. A second way which may improve the method is to perform a sensitivity (or robustness) study on each acoustic signature.

The good correlation between the evolution of internal variables and acoustic emission confirms the physical meaning of these variables and validates the model assumptions (in particular, damage in this type of composite structures can be decomposed in elementary degradation modes as presented in the expression of the thermodynamic potential whose expression is obtained by the means of the tensorial functions representation theory). On the other hand, the simulation of damage evolution could be a way to identify the acoustic events: Chou et al. [42] show that acoustic emission is capable of recording accumulation of damage events in composite pressure vessel but cannot distinguish the various damage modes. The association of experimental acoustic signals and a reliable damage model can thus be seen as a complementary tool to understand the degradation scenario of wound composite structures and the meaning of the recorded acoustic events, in addition to optical observations (micrography, X-ray,…). The satisfactory correlation between acoustic emission and damage evolution also opens the way to an identification procedure for the damage model parameters based on the use of acoustic activity recorded during tensile tests performed on elementary composite samples.

ACKNOWLEDGEMENTS

This work was supported by the French National Research Agency (ANR) through Hydrogène et Piles à Combustible (Project OSIRHYS IV, ANR-09-HPAC-010).

REFERENCES

1. Z. Hashin, Failure criteria for uni-directional fibre composites, Journal of Applied Mechanics, vol. 47, no. 1, pp. 329–334,1980

2. S. W. Tsai and E. Wu, A general theory of strength for anisotropic materials, Journal of Composite Materials, vol. 5, pp. 58–72, 1971

3. P. Xu, J.Y. Zheng, P.F. Liu, Finite element analysis of burst pressure of composite hydrogen storage vessels, Materials & Design, vol. 30, p.2295-2301, 2009

4. L. Kachanov, On the time to failure under creep conditions, *Izv AN SSSV*, vol. 31, pp. 8 – 31, 1958.

5. J. Chaboche, Continuum Damage Mechanics, parts I and II, Journal of Applied Mechanics, vol. 55, pp. 55 – 59, 1989.

6. D. Krajcinovic, Continuum Damage Mechanics, Applied Mechanics Revue, vol. 37, 1984.

7. R. Talreja, S. Yalvac, L.D. Yats, D.G. Wetters, Transverse cracking and stiffness reduction in cross ply laminates of different matrix toughness, Journal of Composite Materials, vol. 26, p.1644-1663, 1992.

8. S. Blassiau, Modelisation des phenomenes microstructuraux au sein d'un composite unidirectionnel carbone/epoxy et prediction de durée de vie: controle et qualification de reservoirs bobinés, PhD thesis, Mines ParisTech, 2005.

9. R. Haj-Ali, H. Kilic, A. Muliana, Nested nonlinear micromechanical and structural models for the analysis of thick-section composite materials and structures, Composites Science and Technology, vol. 67 (10), p.1993-2004, 2007

10. G. Lubineau, P. Ladeveze, An enhanced mesomodel for laminates based on micromechanics, Composite Science and Technology, vol. 62, p.533–541, 2002

11. E. Abisset, F. Daghia, P. Ladevèze, On the validation of a damage mesomodel for laminated composites by means of open-hole tensile tests on quasi-isotropic laminates, Composites Part A, vol. 42, p.1515–1524, 2011.

12. M. Benamira, C. Hochard, A. Haiahem, Behaviour to failure of fibre mat reinforced composite under combined loading conditions, Composites Part B, vol. 42(6), p.1412–1419, 2011.

13. C. Hochard, Y. Thollon, A generalized damage model for woven ply laminates under static and fatigue loading conditions, International Journal of Fatigue, vol. 32(1), p.158–165, 2010.

14. P. Ladevèze, O. Allix, L. David, A mesomodel for localisation and damage computation in laminates, Computer Methods in Applied Mechanics and Engineering, vol. 183, p.105–122, 2000.

15. Y. Thollon, C. Hochard, A general damage model for woven fabric composite laminates up to first failure, Mechanics of Materials, vol. 41, p.820–827, 2009

16. F. Laurin, N. Carrère, J.-F. Maire, A multiscale progressive failure approach for composite laminates based on thermodynamical viscoelastic and damage models, Composites Part A, vol. 38 (1), p.198–209, 2007.

17. P. D. Soden, M.J. Hinton, A.S. Kaddour, A comparison of the predictive capabilities of current failure theories for composite laminates, Composite Science and Technology, vol. 58, p.1225–1254, 1998.

18. M.J. Hinton, A.S. Kaddour, P.D. Soden, A comparison of the predictive capabilities of current failure theories for composite laminates , judged against experimental evidence. Composites Science and Technology, vol. 62, p.1725–97, 2002

18. J. Lemaitre, R. Desmorat, Engineering Damage Mechanics , Springer, 2005

20. D. Eitzen, H.N. Wadley, Acoustic emission: Establishing the fundamentals. Journal of Research of the National Bureau Of Standards, vol. 89,p.75–100, 1984.

21. ST Kim, YT Lee, Characteristics of damage and fracture process of carbon fiber reinforced plastic under loading-unloading test by using AE method, Materials Science and Engineering A, vol. 234, p.322-326, 1997

22. O. Ceysson, M. Salvia, L. Vincent, Damage mechanisms characterisation of carbo fibre / epoxy composite laminates by both electrical resistance measurements and acoustic emission analysis, Scripta Materialia, Vol. 34, pp. 1273-1280, 1996

23. DS de Vasconcellos, F. Touchard, L. Chocinski-Arnault, Tension–tension fatigue behaviour of woven hemp fibre reinforced epoxy composite: A multi-instrumented damage analysis, International Journal of Fatigue, vol. 59, p.159–169, 2014

24. J.J. Scholey, P.D. Wilcox, M.R. Wisnom, M.I. Friswell, Quantitative experimental measurements of matrix cracking and delamination using acoustic emission. Composites Part A, vol. 41, p.612-623, 2010.

25. SE Mechraoui, A. Laksimi, S. Benmedakhene, Reliability of damage mechanism localisation by acoustic emission on glass/epoxy composite material plate, Composite Structures, vol.94, p.1483-1494, 2012

26. R. Yang, Y. He, H. Zhang, Progress and trends in nondestructive testing and evaluation for wind turbine composite blade, Renewable and Sustainable Energy Reviews, vol. 60, p.1225–1250, 2016

27. J. Tang, S. Soua, C. Mares, TH Gan, An experimental study of acoustic emission methodology for in service condition monitoring of wind turbine blades, Renewable Energy, vol.99, p.170-179, 2016

28. N. Godin, S. Huguet, R. Gaertner, L. Salmon, Clustering of acoustic emission signals collected during tensile tests on unidirectional glass/polyester composite using supervised and unsupervised classifiers, NDT&E International, vol.37, p. 253–264, 2004

29. N. Godin, S. Huguet, R. Gaertner, Integration of the Kohonen's self-organising map andk-means algorithm for the segmentation of the AE data collected during tensile tests on cross-ply composites, NDT&E International, vol.38, p.299–309, 2005

30. N. Godin, S. Huguet, R. Gaertner, Influence of hydrolytic ageing on the acoustic emission signatures of damage mechanisms occurring during tensile tests on a polyester composite: Application of a Kohonen's map, Composite Structures, vol.72, p.79–85, 2006

31. HR Mahdavi, GH Rahimi, A. Farrokhabadi, Failure analysis of (±55°) filament-wound pipes using acoustic emission technique, Engineering Failure Analysis, vol.62, p.178–187, 2016

32. S. Blassiau, A. Thionnet, A.R. Bunsell, Micromechanisms of load transfer in a unidirectional carbon fibre-reinforced epoxy composite due to fibre failures: Part 3. Multiscale reconstruction of composite behaviour, Composite Structures, vol. 83, p.312–323, 2008

33. J.P. Berro Ramirez, D. Halm, J.C. Grandidier, S. Villalonga, A fixed directions damage model for composite materials dedicated to hyperbaric type IV hydrogen storage vessel – Part I: model formulation and identification, International Journal of Hydrogen Energy, vol. 40, p. p.13165-13173, 2015

34. A. Lemascon, "Contrôle des matériaux composites par émission acoustique", CETIM, 1993

35. J.P. Berro Ramirez, D. Halm, J.C. Grandidier, S. Villalonga, F. Nony, 700 bar type IV high pressure hydrogen storage vessel burst - simulation and experimental validation, International Journal of Hydrogen Energy, vol. 40, p.13183-13192, 2015

36. J.P. Boehler, Anisotropic constitutive equations for continous media, Journal de mécanique, vol. 17 (2), pp. 153 – 190, 1978.

37. R. Bargellini, D. Halm, A. Dragon, Modelling of anisotropic damage by microcracks: towards a discrete approach, Archives of Mechanics, vol. 58(2), pp. 93 – 123, 2006.

38. D. Halm, A. Dragon, Y. Charles, A modular damage model for quasi-brittle solids – interaction between initial and induced anisotropy, Archives of Applied Mechanics, vol. 72, p.498–510, 2002.

39. J.P. Berro Ramirez, D. Halm, J.C. Grandidier, Deterministic vs. probabilistic burst prediction of wound composite pressure vessel, 9th International Conference on Composite Science and Technology, 2013.

40. J.P. Berro Ramirez, D. Halm, J.C. Grandidier, S. Villalonga, F. Nony, Experimental study of thermo mechanical behavior of wound notched structures, International Journal of Hydrogen Energy, vol. 40, p.13148-13159, 2015.

41 M. Bertin, Fatigue thermomécanique de multicouches polymère/composite, PhD Thesis, ENSMA, 2011.

42. H.Y. Chou, A.P. Mouritz, M.K. Bannister, A.R. Bunsell, Acoustic emission analysis of composite pressure vessels under constant and cyclic pressure, Composites Part A, vol. 70, p.111-120, 2015